



Application of Gaussian Process Estimation for Magnetic Field Mapping

Stefan Hensel¹, Marin B. Marinov² , Tino Schwilk¹, and Dimitar Nikolov²

¹ Department for Electrical Engineering, University of Applied Sciences Offenburg, Badstraße 24, 77652 Offenburg, Germany

² Department of Electronics, Technical University of Sofia, 8, Kliment Ohridski Blvd., 1756 Sofia, Bulgaria
mbm@tu-sofia.bg

Abstract. The applicability of characteristics of local magnetic fields for more precise determination of localization of subjects and/or objects in indoor environments, such as railway stations, airports, exhibition halls, showrooms, or shopping centers, is considered. An investigation has been carried out to find out whether and how low-cost magnetic field sensors and mobile robot platforms can be used to create maps that improve the accuracy and robustness of later navigation with smartphones or other devices.

Keywords: Autonomous navigation · Gaussian processes · Localization and mapping · Machine learning · Magnetic field sensors · ROS · SLAM

1 Introduction

While the outdoor location of objects has been determined a long ago by a combination of satellite navigation and inertial sensors, precise positioning inside buildings remains a subject of active research. In laboratories for measurement and sensor technologies, cost-effective sensors are being studied to reduce or prevent the inevitable drift of inertial navigation.

The naturally occurring geomagnetic field is partly massive distorted in buildings [1]. The distortion is caused by the construction materials and furnishing used [2, 3]. These disturbances of the magnetic flux density \vec{B} are locally clearly expressed and largely stationary. They can, therefore, be used as a characteristic for position determination [4, 5]. Pre-calibrated magnetic field sensors measure these characteristics and use them in the navigation process [6, 7].

The data provided by the sensors is made available to the user in the form of a map [8]. The described project examines how these maps can be produced using mobile robots. Special attention is paid to bringing together several separately created maps so that either a swarm of robots can be deployed or a single robot can create the maps in multiple runs.

2 Methodology

For the given problem, map creation was split into two parallel sub-processes. The position of the robot is determined by the fusion of inertial sensors, i.e. acceleration and rotation rate sensors, with odometry data and the distance data from a depth-sensing camera. The algorithm used is a particle filter that enables simultaneous localization and mapping (SLAM), providing as output data the position and a two-dimensional raster map of the environment. The magnetic field map is calculated using this position and the measurements from commercially available magnetic field sensors.

The map generation process must take into account the uncertainty of the position due to environmental influences and noisy sensors. The magnetic field sensors are susceptible to interferences which can cause a high degree of uncertainty. Since the data from the sensor are discrete and are on trajectory traveled by the robot, interpolation, and extrapolation of these data must be performed. The task of mapping with limited amounts of data is represented in Fig. 1 as an example of the considered two-dimensional case.

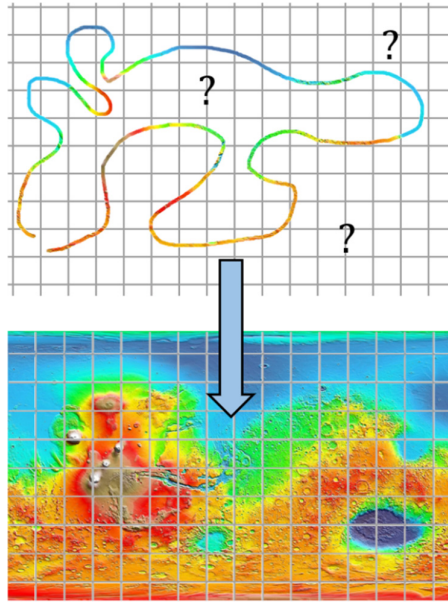


Fig. 1. Prediction of the magnetic flux density \vec{B} in unknown areas based on distributed measurements.

For the prediction of these values for the map generation and the processing of the associated uncertainty in the form of covariance, the appropriateness of the Gaussian processes was investigated.

2.1 Gaussian Processes Regression and Interpolation

We use a Gaussian process (GP) to describe distribution over functions. A Gaussian process is a collection of random variables, any finite number of which have a joint Gaussian distribution.

Gaussian processes [9, 10] are considered as a generalization of the multivariate Gaussian distribution. They can be applied for the estimation of continuous and smooth functions that describe measured data.

Let $m(x)$ and $\kappa(x, x')$ be the mean function and covariance function $\kappa(x, x')$ of a real process $f(x)$. A Gaussian process is completely specified by these two functions and it can be written as

$$f(x) \sim GP(m(x), \kappa(x, x')). \tag{1}$$

The mean function can be taken zero for notational simplicity. In our case, the random variables represent the value of the function $f(x)$ at location x .

A special case of the Gaussian Process Regression (GPR), used in the present work, is known in geostatistics as Kriging. Besides, Gaussian processes can be applied to a variety of machine learning problems, interpolation with splines, classification problems, or data prediction. An illustrative example of regression in the case of one, two, and three measurements are shown in Fig. 2.

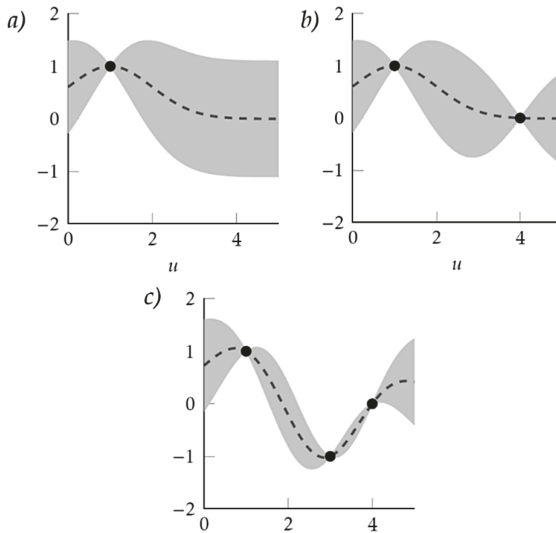


Fig. 2. Principle of Gaussian process regression for a) one measurement, b) two measurements and c) three measurements (adopted from [9])

Measurement points are shown in black, while the grey shaded area gives an interpretation of the so-called 95% confidence interval (twice the standard uncertainty of the estimated function) based on the measured values y_1, y_2, \dots, y_n .

In the GPR applied here, the model functions $f(\mathbf{x})$ are considered/assumed to describe the realizations of a stochastic process whose covariance function $\kappa(\mathbf{x}, \mathbf{x}')$ is given a priori. They are determined by n given uncertain measurements y_1, y_2, \dots, y_n , observed at the points $\mathbf{x}_1, \mathbf{x}_2, \dots, \mathbf{x}_n$. So, the model of the stochastic process can be represented as follows:

$$\begin{aligned} f(\mathbf{x}) &\sim GP(0, \kappa(\mathbf{x}, \mathbf{x}')), \\ y_i &= f(x_i) + \varepsilon_i, i = 1, 2, \dots, n. \end{aligned} \quad (2)$$

The error $\varepsilon(\varepsilon_1, \varepsilon_2, \dots, \varepsilon_n)$ corresponds to white noise. As the measurement- and the a priori models are normally distributed, the estimated a posteriori model will be also normally distributed.

2.2 Selection of the Covariance Function

The selection of a specific covariance function depends on the domain of available knowledge about the underlying process: in the considered case it is related to the behavior of the magnetic field in closed spaces. The problem of the inference requires estimating the parameters of this covariance function using the measurements. Here the parameters are referred to as the so-called hyperparameters; the type of the covariance function is defined a priori in the form of model knowledge. One of the most popular

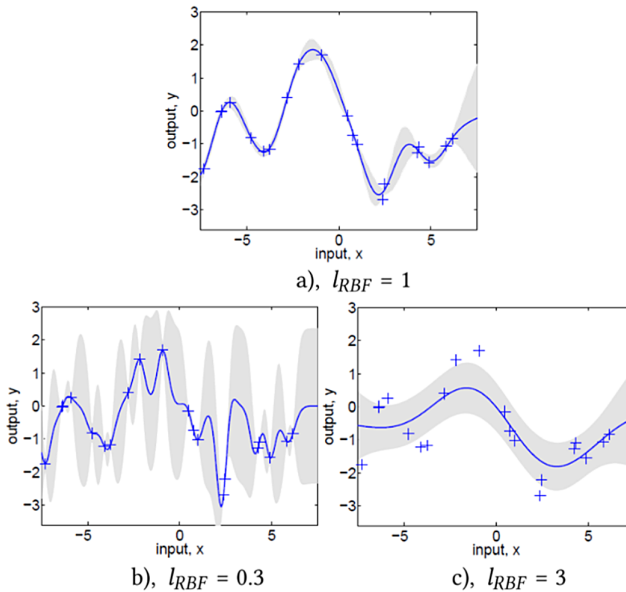


Fig. 3. Influence of the hyperparameters l_{RBF} on the estimation of the covariance function (adapted from [9])

covariance functions is a stationary exponential distribution (the so-called radial basis function RBF) of the form

$$\kappa_{RBF}(\mathbf{x}, \mathbf{x}') = \sigma_{RBF}^2 \cdot \exp\left(-\frac{\|\mathbf{x} - \mathbf{x}'\|^2}{2l_{RBF}^2}\right) \quad (3)$$

where the hyperparameters σ_{RBF}^2 and l_{RBF} express the scale and granularity (bandwidth) of the function.

In Fig. 3 an example of the influence of the hyperparameter l_{RBF} , on the estimated function together with the confidence interval is represented.

The estimation of the hyperparameters on a database is done in the optimal sense by determining the maximum a posteriori probability.

The use of Gaussian processes not only allows the integration of all uncertainties occurring in the mapping but allows the subsequent merging of the created maps based on the estimated accuracy. This is possible by recalculating the map with all measurements or by merging several interpolated maps with weighted arithmetic mean based on covariance recorded at arbitrary times and with any sensors.

3 Experimental Set-up

The basic structure for recording the measurement runs consists of a central host PC on which a ROS kernel runs. Usually, a small Linux netbook is used for this, which sets up a W-LAN network. The individual ROS applications can now be started and monitored from a separate stationary PC. Since it is not necessary to use two separate PCs for this, only one PC was used in the setup pursued here. The magnetic field sensor is connected to the host PC via USB and a breakout board. Both the Turtlebot used and the gamepad required for control are connected to the host PC via USB.

3.1 Hardware

Turtlebot. A mobile robot system of the type Turtlebot was used for the testing. The middleware was the Robot Operating System (ROS) [11], which allows easy driver connection. The ROS is an open-source software environment that provides developers with various libraries and tools to facilitate the development of applications in robotics. Thus, manufacturers distributed numerous hardware elements for which there are device drivers under ROS.

A Turtlebot is a small robot platform in the low price segment. The robot is mostly used for feasibility studies and research purposes because of its flexibility and easy access. It consists of a flat mobile carrying platform, the Kobuki of Yujin Robot, a Kinect of Microsoft as well as a structure that provides space for laptops, other sensors, or constructions.

Inertial Measurement Unit (IMU). The localization of the system was implemented using a g-mapping SLAM algorithm [12]. The three-axis-MEMS magnetic field sensor

HMC5883L is used to record the magnetic field; it can be found, for instance, in smart-phones. Besides, a complete IMU consisting of a three-axis rotation rate sensor and three-axis acceleration sensor is integrated into the chip. By the calculated position of the system, the IMU allows to obtain the projection of the three-dimensional magnetic field measurement into a global coordinate system and thus, to determine the flux density components $\vec{B} = (B_X, B_Y, B_Z)^T$.

There is another advantage of the IMU: depending on the application, part of the data processing, and the signal processing can be transferred from the IMU to an ATmega328 microcontroller. The resolution of the magnetic field sensor is $0.5 \mu\text{T}$ with a measurement range of $\pm 800 \mu\text{T}$ and a deviation of $0.2 \mu\text{T}$.

Figure 4 shows the robot used and the experimental setup with a computer and magnetic field IMU sensor.



Fig. 4. Mobile robot platform (left) and experimental setup combined with magnetic field sensor IMU (right).

For later tests, additional floor markings were made in order to have clues for assessing the position recognition of the turtle bot in the event of multiple measurement runs. Since it was necessary to start measurements from an identical starting point for some series of measurements, a starting field that could be attached to the ground was designed.

3.2 Software

To estimate the parameters of a Gaussian process, complex optimization methods are needed, which usually require $O(n^3)$ operations. As there are hundreds to thousands of measured values at disposal, approximate methods were used to interpolate the magnetic field; the constructed function is known as a measurement function of the magnetic field. Gaussian noise was a priori assumed in the measurement function, the covariance was fixed a priori by the Matérn-function; the latter is a generalized version of RBF and contains an additional hyperparameter for determination of smoothness [13, 14]. The calculation was performed offline in the batch process, i.e. for the entire data set after the measured values were recorded. The input data are magnetometer measurements \vec{B}

along with the position, orientation, and covariance matrix determined by the SLAM algorithm.

Data Preprocessing. The magnetic flux density $\vec{B} = (B_X, B_Y, B_Z)^T$ was measured in x , y , and z direction. To clean up the signal of measurement noise and single outliers, for the time being, it was smoothed by a median filter of 5th order. Since the magnetic field cannot change very quickly due to the limited speed of the Turtlebot, the measurements were subsequently smoothed by moving average filter after rejecting outliers with a median filter of 5th order.

The size of the kernel varies between measurements and must be periodically adjusted. For a large part of the experimental measurements, in case the investigated magnetic field is very irregular, a kernel of size $n \approx 100$ was chosen. In areas where there is a homogeneous magnetic field and there are only separate regions in which the magnetic field strongly fluctuates, the filter kernel has to be reduced in size, so as not to completely remove the measurements.

The IMU and the odometry of the Turtlebot use different sampling frequencies, and the measurements have to be put into correspondence, i.e. to be synchronized, even though they already have a common timestamp by ROS [15].

A magnetic flux density \vec{B} and a time t should be assigned to a point in the x, y plane:

$$\vec{B} = \vec{B}(x_m, y_m, t_m), \quad (4)$$

where x_m, y_m represent the points where the Turtlebot was at the time t_m .

For the assignment and adaptation to the different sampling times, the measurements of the individual topics with a common new sampling time are linearly interpolated. Then they are shifted so that all the measurements are completely synchronous. However, since the position of the magnetic field sensor was centered in the Turtlebot and thus, shifted to the IMU, the position had to be additionally corrected.

A layout regarding the positioning of the magnetic field sensor on the Turtlebot can be found in Fig. 5. In this case

$$\varphi_{sens} = \arctan\left(\frac{x_{dist}}{y_{dist}}\right), d_{sens} = \sqrt{x_{dist}^2 + y_{dist}^2}, \quad (5)$$

The corrected pair of values \bar{x} and \bar{y} is calculated using the relationships

$$\begin{aligned} \tilde{x} &= x + \cos(\varphi + \varphi_{sens})d_{sens} \\ \tilde{y} &= y + \sin(\varphi + \varphi_{sens})d_{sens}, \square \end{aligned} \quad (6)$$

where φ represents the current orientation of the Turtlebot.

To determine the angle φ for each position of the Turtlebot, the orientation of the latter is evaluated using quaternions. For the computation of the three Euler angles (*Roll* Φ , *Pitch* Θ , *Yaw* Ψ) from the quaternions (q_1, q_2, q_3, q_4) the following relationships are used:

$$\begin{bmatrix} \Phi \\ \Theta \\ \Psi \end{bmatrix} = \begin{bmatrix} \text{atan 2}(2(q_0q_1 + q_2q_3), 1 - 2(q_1^2 + q_2^2)) \\ \text{asin}(2(q_0q_2 - q_1q_3)) \\ \text{atan 2}(2(q_0q_3 + q_1q_2), 1 - 2(q_2^2 + q_3^2)) \end{bmatrix} \quad (7)$$

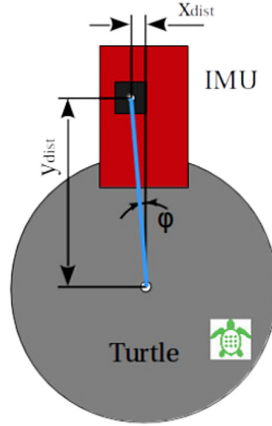


Fig. 5. The distance of the magnetic field sensor to the center of the Turtlebots

The angle φ corresponds to the pitch angle Θ . For greater clarity further on in this work, the coordinates of the magnetic field sensor are denoted by x and y instead \tilde{x} and \tilde{y} .

With these transformations, it is possible to map the magnetic field measurements in the localization frame of the robot. These data are fused with the robot localization based on laser scan data and odometry. To get the robot trajectory we employ a classical particle filter-based localization and mapping algorithm (SLAM), based on [12]. This not only results in a trajectory driven by the robot but also in an uncertainty estimation of the actual position, which is expressed with the covariance matrix

$$\sigma_{max}^2 = \max \left(\begin{bmatrix} \sigma_{x,x}^2 & \sigma_{x,y}^2 \\ \sigma_{y,x}^2 & \sigma_{y,y}^2 \end{bmatrix} \right) \quad (8)$$

An exemplary result for the trajectory is shown in Fig. 6. The associated uncertainty is visualized with an ellipse based on the actual covariance.

Mapping. To create a magnetic field map from the driven path, different interpolation methods exist. Matlab offers the function *griddata* for the interpolation of functions $f(x, y)$ via a previously defined grid. The method used here is based on Delaunay triangulation, i.e. triangles are formed between pairs of points in space. These triangles are chosen to avoid long thin triangles. Since the triangles cover the entire grid and do not overlap, a value can be assigned to each point on the grid.

Multimap Data Fusion. To generate a map from several series of measurements, a fusion of the measured values is necessary. These can be performed either by running an environment multiple times with a single robot only or by running simultaneously more robots in the environment. In the case of interpolation with Gaussian processes this fusion is easily realized. All measurements with an associated uncertainty can be added to the Gaussian process as training data. The resulting interpolation is already weighted and based on a distribution function. It makes no difference whether the same

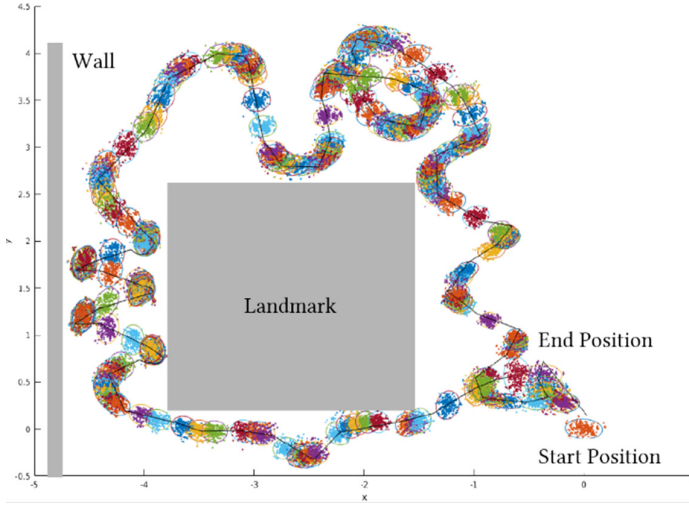


Fig. 6. Base data for data fusion of several maps, showing coordinates and associated magnetic field measurements and their estimated uncertainty.

point is traversed several times during measurement, or whether several measurements are fused. The consequence in both cases is that inaccuracies or measurement errors are less weighted in the resulting map.

In the case of classical interpolation, such an approach would not lead to the correct result, since each value enters the result with the same weight.

To fuse several maps according to their uncertainty, an uncertainty value σ is assigned to each geometric point \tilde{P} , in addition to a value z_{mag} which expresses the magnetic field strength at the positions x and y . This is depicted in Fig. 7 and follows the equation

$$\tilde{P}_{map} = \tilde{P}_{map}(x, y, z_{mag}, \sigma). \tag{9}$$

To associate appropriate weights to the individual measured values, an engineering approach is used.

It is assumed that the measurement of the magnetic field at the location \tilde{P} is highly uncertain especially when the positional covariance is particularly great. A measured value has, therefore, a large influence on the result, only in case, the Turtlebot was there with a high degree of certainty.

For this purpose, the maximum value

$$\sigma_{max}^2 = \max \left(\begin{bmatrix} \sigma_{x,x}^2 & \sigma_{x,y}^2 \\ \sigma_{y,x}^2 & \sigma_{y,y}^2 \end{bmatrix} \right) \tag{10}$$

of the already known covariance matrix from the SLAM algorithm of the localization, a module is used.

Thus, a very small σ_{max} stands for very good position detection, i.e. for very accurate measurement of the magnetic field. Several N maps $P_{map,i}$ with i from 1 to N are now

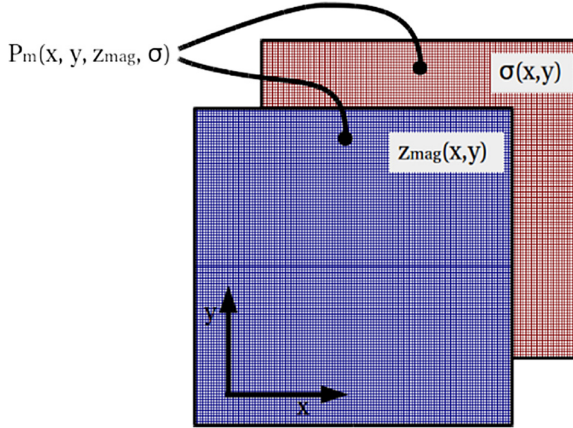


Fig. 7. Base data for data fusion of several maps, showing coordinates and associated magnetic field measurements and their estimated uncertainty.

calculated to form a map P_{map} , using the following equation:

$$P_{map}(x, y) = \sum_{i=1}^N \left(\frac{z_i(x, y)}{\sigma_i^2(x, y)} \right) / \left(\frac{1}{\sigma_{max}^2(x, y)} \right). \tag{11}$$

It shows that a value of 0 is not permitted for the uncertainties. In a real process this indeed never occurs. Nevertheless, such a measurement can be skipped, so that at this point the map is showing a gap in the measurements.

If measurements that tightly cover the entire area in space are available, the map fusion can be performed using a weighted average. The advantage of this map fusion compared to the Gaussian processes is the lower computational load. However, the acquisition of the measured data with sufficient density is a fundamental problem: for this purpose, an intelligent interpolation and extrapolation of the measured values cannot be ruled out [16].

4 Experimental Results

In this section, selected experiments are presented and the results obtained from them are briefly discussed.

4.1 Mapping Procedure - Approach

Since the magnetic flux density \vec{B} is a vector field $\vec{B}(x, y) = (B_x, B_y, B_z)^T$, but only one scalar can be interpolated over x and y , some considerations have to be made.

It is conceivable to interpolate every one of the measured components of \vec{B} . In the further course the measured values of B_x are described with $M_{B_x}(x, y)$. Similarly,

the description of B_y and B_z . A two-dimensional interpolation of $M_{B_x}(x, y)$ results in $M_{I,B_x}(x, y)$

$$\begin{aligned} M_{B_x}(x, y) &\xrightarrow{\text{interpoliert}} M_{I,B_x}(x, y), \\ M_{B_y}(x, y) &\xrightarrow{\text{interpoliert}} M_{I,B_y}(x, y), \\ M_{B_z}(x, y) &\xrightarrow{\text{interpoliert}} M_{I,B_z}(x, y). \end{aligned} \quad (12)$$

From these three interpolated maps, it is now possible to generate a map of the absolute value $M_{I,abs(B_x,B_y,B_z)}(x, y)$. For this, however, it is necessary to refer the values to a global coordinate system. Since the Turtlebot can only rotate around the z-axis, the necessary transformation results

$$M_{B_y}(x, y) = R(\varphi) \cdot \bar{M}_{B_x}(x, y). \quad (13)$$

Here, R is the rotation matrix as a function of the orientation angle φ of the Turtlebot:

$$\mathbf{R} = \begin{bmatrix} \cos(\varphi) & -\sin(\varphi) & 0 \\ \sin(\varphi) & \cos(\varphi) & 0 \\ 0 & 0 & 1 \end{bmatrix} \quad (14)$$

The absolute value for B_x , B_y and B_z is given by

$$M_{I,abs(B_x,B_y,B_z)}(x, y) = \sqrt{M_{I,B_x}(x, y)^2 + M_{I,B_y}(x, y)^2 + M_{I,B_z}(x, y)^2} \quad (15)$$

4.2 Experimental Runs

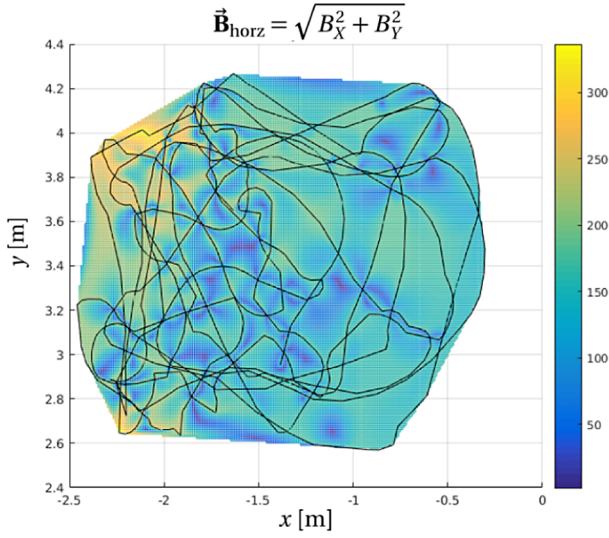
Experimental runs in several environments have proven small to little influence of the magnetic field vector B_z for the sensitivity of the overall field strength. This is due to the considered scenarios, where the robot is mainly operating in industrial or home environments, where the ceiling is too far away to have any influence, and commonplace objects rather extend to the floor and thus permit to drive under. Therefore, the vertical magnetic component can be omitted, which significantly speeds up the interpolation and combination of the measured data. The overall field strength for B_x and B_y is given by

$$M_{I,abs(B_x,B_y)}(x, y) = \sqrt{M_{I,B_x}(x, y)^2 + M_{I,B_y}(x, y)^2} \quad (16)$$

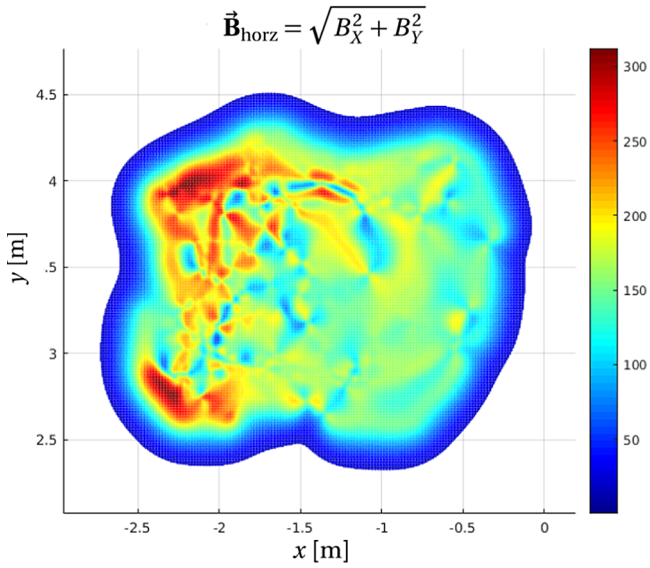
In an initial study, the suitability of Gaussian processes for interpolating measured data was examined. For comparison, we applied the classical two-dimensional linear interpolation. Although the latter cannot be used for covariance indication and evaluation, the computation time is several orders of magnitude smaller.

However, it quickly becomes clear what qualitative advantage can be achieved by interpolation and prediction with Gaussian processes. Figure 8(a) shows the linear interpolation based on the trajectory traveled, which is plotted in black. The result of the GP for the same record is shown in Fig. 8(b).

Magnetic maps were recorded based on several test runs in different areas of the university. Figure 9 illustrates the qualitative results for a small area of a laboratory.



a) result obtained by linear interpolation



b) result of Gaussian processes

Fig. 8. Created map of the horizontal flow density

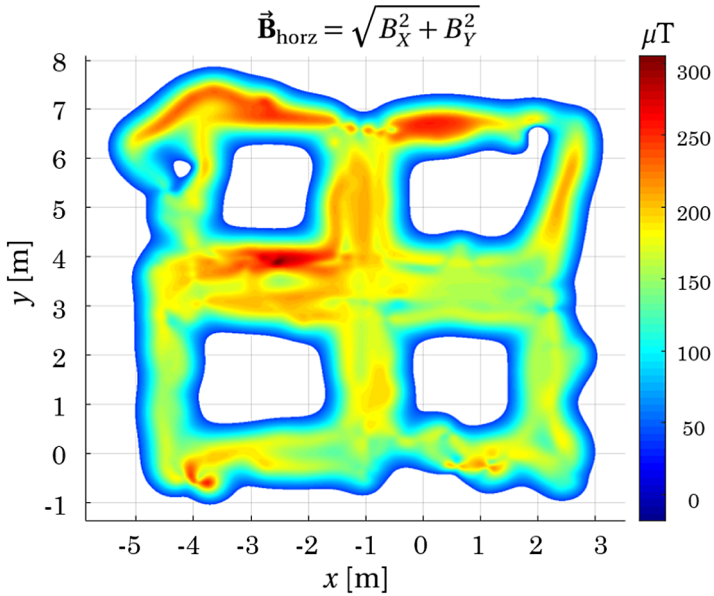


Fig. 9. Illustrative map of the horizontal flow of the laboratory for measuring and sensor technology

5 Conclusions

The investigation shows that the Gaussian regression is fundamentally suitable for producing a complete and usable map (of continuous features) from individual measurements. The maps created have a good degree of detail. The advantages compared to less expensive methods lie in the simple integration of new measurements, the availability

of a quality measure in the form of a covariance matrix, and, based thereon, natural integration into stochastic localization methods. The modeling also allows the introduction of boundary conditions and model knowledge. However, all this is at the expense of extensive calculations.

The maps were created with a resolution of 5 cm, the potential for a positioning accuracy is within a few decimeters to meters, which is already sufficient for the continuous improvement and drift correction of inertial sensors.

Acknowledgments. This research is supported by the Bulgarian National Science Fund in the scope of the project “Exploration the application of statistics and machine learning in electronics” under contract number KII-06-H42/1.

References

1. Saxena, A., Zawodniok, M.: Indoor positioning system using geomagnetic field. In: IEEE International Instrumentation and Measurement Technology Conference (I2MTC) Proceedings, Montevideo, Uruguay (2014)
2. Iatcheva, I.I., Andreev, A.D., Stancheva, R.D., Lilyanova, I.T.: Electromagnetic flow meter field distribution maximizing device sensitivity. *Mater. Sci. Forum* **856**, 157–162 (2016)
3. Shockley, J.A., Raquet, J.F.: Navigation of Ground vehicles using magnetic field variations. *Navigation* **61**, 237–252 (2014)
4. Li, B., Gallagher, T., Dempster, A., Rizos, C.: How feasible is the use of magnetic field alone for indoor positioning? In: Proceedings of the International Conference on Indoor Positioning and Indoor Navigation (IPIN), Sydney, Australia (2012)
5. Hensel, S., Marinov, M.B., Schmitt, M.: System setup for synchronized visual-inertial localization and mapping. In: 2020 XXIX International Scientific Conference Electronics (ET), Sozopol, Bulgaria (2020)
6. Frassl, M., Angermann, M., Lichtenstern, M., Robertson, P., Julian, B., Doniec, M.: Magnetic maps of indoor environments for precise localization of legged and non-legged locomotion. In: Proceedings of the IEEE/RSJ International Conference on Intelligent Robots and Systems (IROS), Tokyo, Japan (2013)
7. Filipov, F.: Forschung und Implementierung von Technologien für die Navigation in Innenräumen, Sofia: Dissertation, Technische Universität Sofia (2016)
8. Kim, H.S., Seo, W., Baek, K.R.: Indoor positioning system using magnetic field map navigation and an encoder system. *Sensors* **17**(3), 651 (2017)
9. Rasmussen, C.E., Williams, C.K.I.: *Gaussian Processes for Machine Learning*. MIT Press, Cambridge (2006)
10. Jain, A., Nghiem, T., Morari, M., Mangharam, R.: Learning and control using gaussian processes. In: 2018 ACM/IEEE 9th International Conference on Cyber-Physical Systems (ICCPs), Porto, Portugal (2018)
11. Quigley, M., Gerkey, B., Smart, W.: *Programming Robots with ROS*. O’Reilly Media, Sebastopol (2015)
12. Grisetti, G., Stachniss, C., Burgard, W.: Improved techniques for grid mapping with rao-blackwellized particle filters. *IEEE Trans. Rob.* **23**, 34–46 (2007)
13. Minasny, B., McBradley, B.: Spatial prediction of soil properties using EBLUP with the Matérn covariance function. *Geoderma* **140**, 323–456 (2007)
14. Hensel, S., Marinov, M.B.: Estimation of magnetic field maps with mobile platforms. In: Proceedings of the 7th FDIBA Conference, Sofia, 30 November–1 December 2017

15. Kokolanski, Z.: Hardware techniques for improving the calibration performance of direct resistive sensor-to-microcontroller interface. *Metrol. Meas. Syst.* **20**(1), 529–542 (2013)
16. Klein, L.: *Sensor and Data Fusion*. SPIE-International Society for Optical Engineering, Washington (2004)